IET Journals
IET Electric Power Applications

Low-speed performance comparisons of back-EMF detection circuits with position-dependent load torque

H.-C. Chen   T.-Y. Tsai   C.-K. Huang*

Department of Electrical and Control Engineering, National Chiao Tung University, Hsinchu, Taiwan, Republic of China
*Also an associate researcher in the Energy and Environment Laboratories, Industrial Technology Research Institute, Hsinchu, Taiwan, Republic of China
E-mail: hcchen@mail.nctu.edu.tw

Abstract: Because of the widely used brushless DC motors (BDCMs) in high-efficiency variable-speed compressors, many sensorless controls with square-wave operation had been developed in the literatures. Recently, more and more low-production-cost BDCM-type compressors with position-dependent load torque, such as rotary compressors, are applied to the residential products, which lead to the importance of low-speed performance of sensorless control. The authors address the low-speed performance comparisons between two common back-EMF detecting circuits (BEDCs). Without using the actual refrigerant system, a Motor-Generator set coupled with a disk and copper cylinder are also built up to serve as the experimental position-dependent load torque. From the simulated and experimental results, one of the BEDCs is better than the other one for the low-speed application of position-dependent load torque.

1 Introduction

Because of the rotor permanent-magnetic field, brushless DC motors (BDCMs) possess higher efficiency than the popular induction motors (IMs). Additionally, for variable-speed IMs, only relatively sinusoidal-current operations can be used to maintain efficiency. But in the control of variable-speed BDCMs, square-wave current with rich harmonic currents can be drawn without the loss of high efficiency. Therefore more and more BDCMs are used in high-efficiency residential applications – variable-speed refrigerant systems, including compressor motors and fan motors.

In the normal operations of BDCMs, the discrete rotor positions should be monitored by the mounted position sensors to yield adequate current commutations. However, in refrigerant system, the temperature in the hermetic compressors is usually more than 90 °C, which would result in the failures of Hall position sensors. It follows that the sensorless control techniques without position sensors become important in the applications of BDCMs to variable-speed refrigerant systems.

In the last decades, many sensorless controls with square-current operation had been proposed in the literature and they can be divided into several groups [1]. The group of back-EMF detecting methods commutates the winding currents according to the detected rotor positions from the back-EMF detecting circuits (BEDCs) because the rotor position can be found from the back-EMFs of BDCMs and back-EMFs can be sensed from the terminal voltages of the unexcited phase [2–9].

Based on the frequency responses of passive filters, one type of back-EMF detecting circuit (named BEDC-I) including band-pass and low-pass filters had been proposed in [2–7]. In [2–4], three Y-connected band-pass filters are used to attenuate the dc and high-frequency PWM voltages in the terminal voltages. The position signals are estimated from the comparisons of three filtered signals with their pseudo-neutral signal. In [5, 6], position signals are obtained from the comparisons of two of the three filtered signals. Low-cost back-EMF detecting circuit including only one band-pass filter and using one terminal voltage had been used in [7] to obtain the position signal.

The detailed analysis of band-pass filter and discussion can be found in [5, 6].

Meanwhile, another type of back-EMF detecting circuit (named BEDC-II) with three Y-connected low-pass filters used in [8, 9] can also be found. It is noted that these low-pass filters are used to attenuate the injected noise, rather than to attenuate the PWM voltage components. The position signals can be estimated by comparing the three filtered signals with the filtered DC-link voltage. However, in BEDC-II, the feedback position signals with PWM fluctuations cannot be directly used to commutate the motor currents. Therefore a complicated phase shift function should be implemented in the BEDC-II's commutating signal generator with integrated circuit [8] and MCU/DSP [9].

Recently, because of the low-cost trend of high-efficiency variable-speed refrigerant products, low-production-cost rotary compressors are widely used in the residential applications. From the view of load characteristics, the rotary compressor possesses position-dependent load torque [10, 11] where its maximum load torque in specific position may be near four times its minimum load torque. It follows that the instantaneous speed of BDCM fluctuates around its average speed. Unfortunately, this speed deviation becomes relatively large, especially at low speed, which would introduce disparate position errors to BEDCs and degrade the low-speed performance of the sensorless control.

In fact, compressor motors in variable-speed refrigerant products run at low speed most of the time. That is, the low-speed performance of sensorless BDCMs control is more important than the high-speed performance. In [12], the high-speed performances of sensorless control with PWM inverter and variable DC-link inverter had been addressed. It shows that the current commutation error resulting from PWM period has a great effect on the high-speed performances of sensorless control. However, no low-speed performance comparisons of sensorless BDCM control can be found in the literatures.

Therefore in this paper, the low-speed performances of two sensorless controls with circuits BEDC-I and BEDC-II are studied and analysed. The result shows that position-dependent load torque would produce significant position-dependent detecting errors, especially at low speed. That is, the low-speed performance of sensorless control is highly related to the induced position-dependent detecting error. The simulation and experiment including both BEDCs and their sensorless controls had been finished. The simulated and experimental data demonstrate the results of analysis.

2 Sensorless BDCM control

Compared with the variable-speed IMs, BDCMs can be controlled with square-wave currents without loss of their efficiencies. Both 120°-conduction method and 180°-conduction method are able to draw square-wave currents and the main difference between them is that there is always one unexcited phase in the former, and no unexcited phase in the latter. Therefore the former is always used in the square-current sensorless controls [2–9, 11–13] for that the motor positions can be known by sensing the zero crossing points (ZCPs) of back-EMFs from the approximations of motor terminal voltage and the BDCM back-EMF in the unexcited phase.

In addition, adjusting the average motor terminal voltages to regulate the motor speed is the simplest variable-speed control of BDCMs in refrigerant systems. By considering the complication of implementation, pulse width modulation (PWM) scheme with six power switches to adjust the average motor terminal voltages is better than the scheme of changing the dc-link voltage because of its extra switch [12].

Therefore the configuration of square-current sensorless control with PWM scheme is illustrated in Fig. 1 where BEDC obtains the position signals H_U, H_V and H_W from the inverter and motor terminal voltages V_P, V_N, V_U, V_V and V_W. By using the above position signals H_U, H_V and H_W, commutation signal H and speed ω_r can be obtained and then, the speed controller tunes the PWM duty ratio adequately according to the speed difference between speed command ω_r^* and the estimated speed ω_r. Then, the switching signal generator yields the six gate signals G_{T1}, G_{T2}, G_{T3}, G_{T4}, G_{T5} and G_{T6} according to the commutation signal H and PWM duty ratio to yield square-wave currents adequately. Voltages e_U, e_V and e_W are the back-EMFs of the two identified BDCMs coupled together.

Four common 120° square-wave PWMs (SWPWMs) as shown in Fig. 2 can be found in the sensorless BDCM control where only upper or lower switch of one leg is conducting with PWM. The 120° SWPWMs from Fig. 2a–2d are named fully upper PWM (FUPWM) [2–7, 11], fully lower PWM (FLPWM) [13], alternatively leading PWM (ALeadPWM) [12] and alternatively lagging PWM (ALagPWM) [8, 9], respectively.

The waveforms of terminal voltages for various SWPWMs can be found in Fig. 2 and all their expressions for various switching-signal states are tabulated in Table 1. The states A, B, C, D, E, F can be found in ALagPWM and the states I, J, K, L, M, N can be found in ALeadPWM. In addition, FUPWM and FDPWM include states A, C, E, J, L, N and states B, D, F, I, K, M, respectively.

3 BEDC-I

BEDC-I is plotted in Fig. 3 where three identical circuit networks are Y-connected and four terminal voltages V_N, V_U, V_V and V_W are used [2–7]. The position signals H_U,
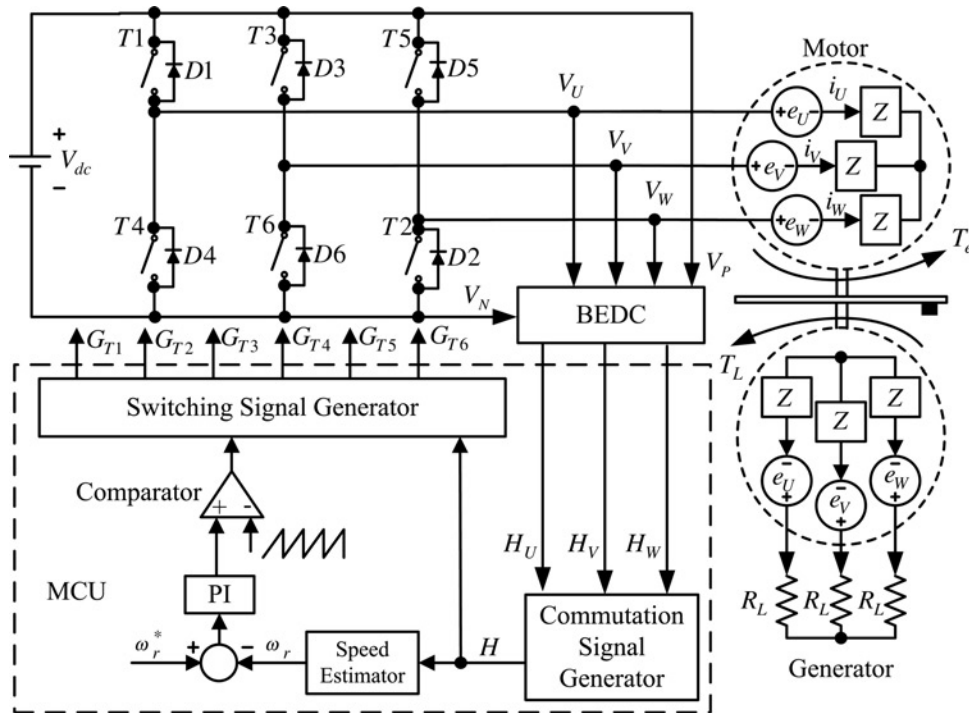
Figure 1 *Configuration of sensorless control with 120° SWPWM*

H_V and H_W are generated from the comparisons between the pseudo-neutral signal v_n and the filtered signals v_U, v_V, v_W, respectively. Since the commutation intervals are 60° electrical degrees in 120° SWPWM, the desired winding current commutation should occur at $(30° + k \times 60°)$ lagging behind the ZCPs of back-EMFs where k is an integer to operate BDCM efficiently. Thus, by using the phase response of circuit networks, BEDC-I is designed to detect the points of 90° lagging behind the ZCPs of back-EMFs.

Figure 2 *120° SWPWMs*

a FUPWM
b FLPWM
c ALeadPWM
d ALagPWM

3.1 Circuit analysis

The individual circuit network can be seen as a low-pass filter cascaded with a band-pass filter where the former provides 90°-delay relation and the latter keeps the signal gain constant during the BDCM speed range from ω_{rlow} through ω_{rhigh} in rpm. when a *P*-poles BDCM operating at ω_r(rpm), the fundamental frequency $f_1 = p\omega_r/120$ (Hz) of back-EMF and terminal voltage is located in the range from f_{low} to f_{high}

$$f_{Low} = \frac{P\omega_{rLow}}{120} \leq f_1 = \frac{P\omega_r}{120} \leq \frac{P\omega_{rHigh}}{120} = f_{High} \qquad (1)$$

To keep near 90° phase shifting during BDCM speed range in (1), the lowest fundamental frequency f_{Low} from the lowest speed ω_{rLow} should be significantly higher than the cut-frequency f_{LP-I} of the low-pass filter

$$f_{Low} \gg f_{LP-I} = \frac{R_{11} + R_{12}}{2\pi R_{11} R_{12} C_{11}} \qquad (2)$$

The frequency response of band-pass filter shown in Fig. 3 can be derived as

$$F_{BP}(jf_1) = \frac{jf_1}{f_{BP1}(1 + jf_1/f_{BP1})} \frac{1}{(1 + jf_1/f_{BP2})} \qquad (3)$$

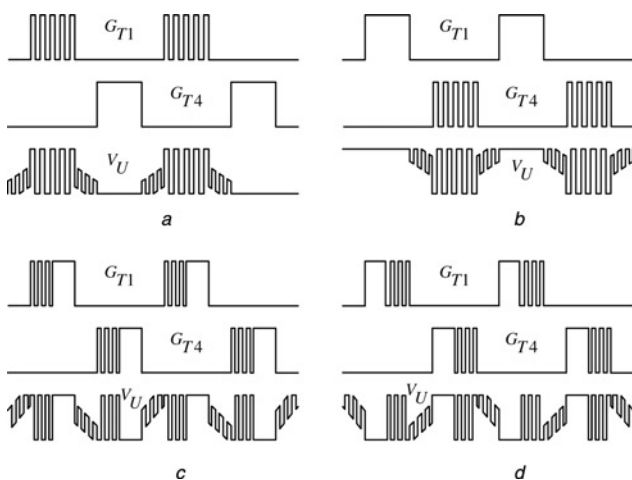where f_{BP1} and f_{BP2} ($<f_{BP1}$) are the corner frequencies of band-pass filter.

Table 1 Expressions of terminal voltages for all switching states

State	Always OFF	Always ON	PWM ON/OFF	V_U	V_V	V_W
A	$G_{T2}\,G_{T3}\,G_{T4}\,G_{T5}$	G_{T1}	G_{T6} ON	V_{dc}	0	$0.5V_{dc} + 1.5e_W$
			G_{T6} OFF	V_{dc}	V_{dc}	$V_{dc} + 1.5e_W$
B	$G_{T3}\,G_{T4}\,G_{T5}\,G_{T6}$	G_{T2}	G_{T1} ON	V_{dc}	$0.5V_{dc} + 1.5e_V$	0
			G_{T1} OFF	0	$1.5e_V$	0
C	$G_{T1}\,G_{T4}\,G_{T5}\,G_{T6}$	G_{T3}	G_{T2} ON	$0.5V_{dc} + 1.5e_U$	V_{dc}	0
			G_{T2} OFF	$V_{dc} + 1.5e_U$	V_{dc}	V_{dc}
D	$G_{T1}\,G_{T2}\,G_{T5}\,G_{T6}$	G_{T4}	G_{T3} ON	0	V_{dc}	$0.5V_{dc} + 1.5e_W$
			G_{T3} OFF	0	0	$1.5e_W$
E	$G_{T1}\,G_{T2}\,G_{T3}\,G_{T6}$	G_{T5}	G_{T4} ON	0	$0.5V_{dc} + 1.5e_V$	V_{dc}
			G_{T4} OFF	V_{dc}	$V_{dc} + 1.5e_V$	V_{dc}
F	$G_{T1}\,G_{T2}\,G_{T3}\,G_{T4}$	G_{T6}	G_{T5} ON	$0.5V_{dc} + 1.5e_U$	0	V_{dc}
			G_{T5} OFF	$1.5e_U$	0	0
I	$G_{T2}\,G_{T3}\,G_{T4}\,G_{T5}$	G_{T6}	G_{T1} ON	V_{dc}	0	$0.5V_{dc} + 1.5e_W$
			G_{T1} OFF	0	0	$1.5e_W$
J	$G_{T3}\,G_{T4}\,G_{T5}\,G_{T6}$	G_{T1}	G_{T2} ON	V_{dc}	$0.5V_{dc} + 1.5e_V$	0
			G_{T2} OFF	V_{dc}	$V_{dc} + 1.5e_V$	V_{dc}
K	$G_{T1}\,G_{T4}\,G_{T5}\,G_{T6}$	G_{T2}	G_{T3} ON	$0.5V_{dc} + 1.5e_U$	V_{dc}	0
			G_{T3} OFF	$1.5e_U$	0	0
L	$G_{T1}\,G_{T2}\,G_{T5}\,G_{T6}$	G_{T3}	G_{T4} ON	0	V_{dc}	$0.5V_{dc} + 1.5e_W$
			G_{T4} OFF	V_{dc}	V_{dc}	$V_{dc} + 1.5e_W$
M	$G_{T1}\,G_{T2}\,G_{T3}\,G_{T6}$	G_{T4}	G_{T5} ON	0	$0.5V_{dc} + 1.5e_V$	V_{dc}
			G_{T5} OFF	0	$1.5e_V$	0
N	$G_{T1}\,G_{T2}\,G_{T3}\,G_{T4}$	G_{T5}	G_{T6} ON	$0.5V_{dc} + 1.5e_U$	0	V_{dc}
			G_{T6} OFF	$V_{dc} + 1.5e_U$	V_{dc}	V_{dc}

$$f_{BP1} = \frac{1}{2\pi C_{12}R_{13}} \qquad (4)$$

$$f_{BP2} = \frac{1}{2\pi C_{13}R_{14}} \qquad (5)$$

To keep the magnitude of the filtered constant during the BDCM speed range, the lowest fundamental frequency f_{Low} should be larger than the corner frequency f_{BP1} and the highest fundamental frequency f_{High} should be smaller than the corner frequency f_{BP2}. On the other hand, the PWM frequency f_{PWM} should be larger than the corner frequency f_{BP2} to attenuate the PWM voltage components
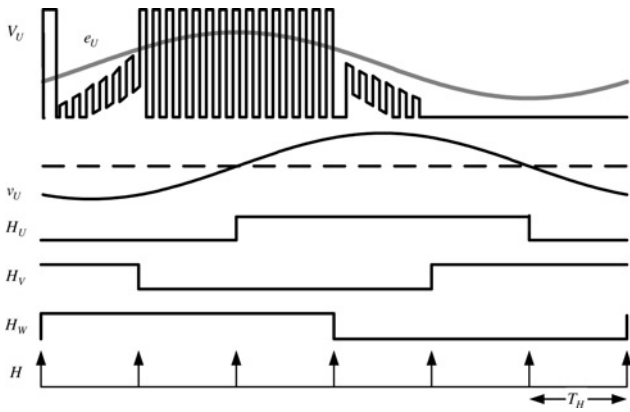

Figure 3 BEDC-I

163
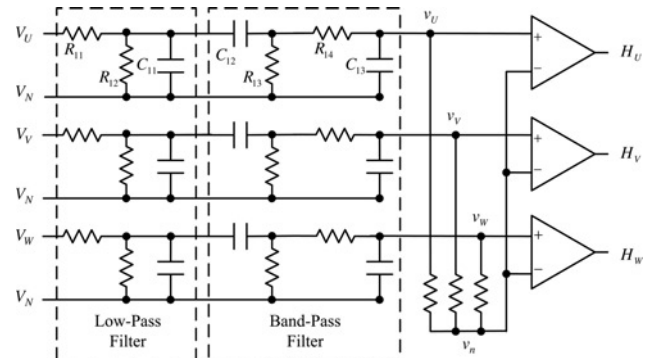
Figure 4 *Illustrated waveforms for BEDC-I with FUPWM*

at the filtered voltages v_U, v_V and v_W. Consequently, the relation of above critical frequencies can be expressed as

$$f_{LP-I} \ll f_{BP1} < f_{Low} \leq f_1 \leq f_{High} < f_{BP2} < f_{PWM} \quad (6)$$

3.2 120° SWPWM

Using various 120° SWPWM in BDCM operation results in various motor terminal voltages as shown in Fig. 2. It is noted that all the various terminal voltages possess the same magnitudes of fundamental and harmonic voltages. Consequently, all four 120° SWPWM in Fig. 2 can be used with BEDC-I because the design of BEDC-I is based on the frequency response of passive filters. Fig. 4 shows the illustrated waveforms of BEDC-I where the filtered signal v_U can be found to be 90° lagging behind the ZCPs of back-EMFs. The position signals H_U, H_V and H_W are square waveforms 120° out of phase with each other. To obtain adequate current commutation, the desired commutation signals H should be generated as shown in Fig. 4.

3.3 Commutation signal generator

From Fig. 4, we can find that the edges of position signals H_U, H_V and H_W occur at the desired commutation instants. Thus, the block diagram of the commutation signal generator is plotted in Fig. 5 where the combined signal H_X is generated from the exclusive-or (XOR) operation of three position signals H_U, H_V and H_W. Then, the commutation signal H can be generated by using the common edge-trigger function. That is, it is easy to
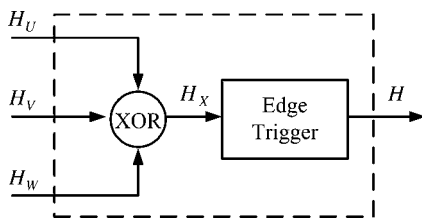

Figure 5 *Commutation signal generator for BEDC-I*

implement the commutation signal generator for BEDC-I by using the general-purpose DSP/MCU [2, 3, 7].

3.4 Position-dependent load torque

For constant load torque, the instantaneous motor speed ω_r in steady state can be seen as constant and equal to its average value $\bar{\omega}_r$. Thus, all harmonic frequencies f_h of terminal voltage are integral multiples of the fundamental frequency f_1 corresponding to the motor speed ω_r.

$$f_h = hf_1 = h\frac{P\omega_r}{120} \quad (7)$$

where h is an odd integer >1. At low speeds, the fundamental frequency f_1 is near the lowest fundamental frequency f_{Low} and thus, the lowest harmonic frequency $3f_1$ may be smaller than the corner frequency f_{BP2} as shown in Fig. 6a. It follows that some low-speed position detection error may occur with constant load torque.

For position-dependent load torque, the instantaneous motor speed ω_r is varying around its steady-state average value $\bar{\omega}_r$. For 2-poles BDCMs, electrical frequency is equal to the mechanical frequency and thus the speed variations due to position-dependent load torque would contribute to the same harmonic frequencies as the case of constant load torque in (7).

However, for multi-pole-pairs BDCMs (even pole number $P > 2$), electrical frequency is $P/2$ times the mechanical frequency and thus, the speed variations due to position-dependent load torque would lead to not only the harmonics f_h in (7) but also the interharmonics f_{ih} in the motor terminal voltages. For P-poles BDCMs (even $P > 2$), the interharmonic frequencies f_{ih} are

$$f_{ih} = hf_1\left(1 \pm \frac{2k}{P}\right) \quad (8)$$

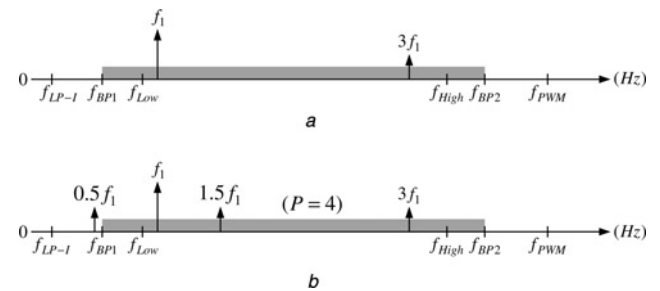where k is an integer from 1 to $P - 1$ except $0.5P$. For example, for a 4-pole BDCM, the induced interharmonic

Figure 6 *Terminal voltage frequency spectrum and relationship between the various frequencies being discussed*

a With constant load torque
b With position-dependent load torque

frequency f_{ih} would be $0.5f_1$, $1.5f_1$, $4.5f_1$ … as shown in Fig. 6b.

Obviously, from (8) and Fig. 6b, some resulting interharmonic frequencies f_{ih} are inevitably located in the frequency band of band-pass filter from f_{BP1} to f_{BP2}. It means that the interharmonic frequencies f_{ih} due to position-dependent load torque cannot be easily attenuated by the band-pass filter and would result in the undesired interharmonics. That is, additional undesired position detection error due to position-dependent load torque will be introduced into sensorless control through BEDC-I, especially at low speed.

4 BEDC-II

From Table 1, when the SWPWM switching state is ON, the terminal voltages of unexcited phase are equal to

$$V_X = 0.5V_{\text{dc}} + 1.5e_X \qquad (9)$$

where X may be U, V and W. t implies that comparing the terminal voltage V_x with half DC-link voltage $0.5V_{\text{dc}}$ is able to detect the ZCPs of back-EMF. Therefore BEDC-II is developed as plotted in Fig. 7 where four identified low-pass filters and all terminal voltages V_P, V_N, V_U, V_V and V_W are used [8, 9].

4.1 Circuit analysis

However, the equality in (9) is satisfied only when the PWM switching signal is ON. To exactly separate the 'ON' duration, the waveforms of terminal voltage must be preserved, not filtered. Therefore it follows that the low-pass filter in BEDC-II is not designed to attenuate the PWM component in the terminal voltage, but to reject the

Figure 7 *BEDC-II*

switching noises. It follows that the cut-frequency $f_{\text{LP-II}}$ of the low-pass filter in BEDC-II must be much larger than PWM frequency f_{PWM}

$$f_{\text{LP-II}} = \frac{R_{21} + R_{22}}{2\pi R_{21} R_{22} C} \gg f_{\text{PWM}} \qquad (10)$$

It is noted that the PWM frequency f_{PWM} for BEDC-I is significantly larger than $f_{\text{LP-I}}$ as shown in (6). Comparing (10) with (6) also shows the main difference of circuit design between BEDC-I and BEDC-II.

To obtain filtered signal v_p from the terminal voltages V_P and V_N, the value of resistor R_{23} must be the sum of the values of R_{21} and R_{22}.

$$R_{23} = R_{21} + R_{22} \qquad (11)$$

4.2 120° SWPWM

From Fig. 2, we can find that the comparisons of the unexcited-phase terminal voltage and half DC-link voltage between commutation instants can be divided into two types. One type initially keeps fixed and then turns to change with PWM frequency until the coming of ZCPs of back-EMFs as shown in the dashed-block of Fig. 8. The other type initially changes with PWM frequency and then keeps fixed after ZCPs of back-EMFs. Using the common edge-trigger function is able to identify the ZCPs of back-EMFs from the former type.

Therefore strictly speaking, all four 120° SWPWM in Fig. 2 can be used with BEDC-II. However, by considering the complication of required edge-trigger function, only ALagPWM in Fig. 2d is suitable for BEDC-II for that all the comparisons are divided into the former types as shown in Fig. 8.
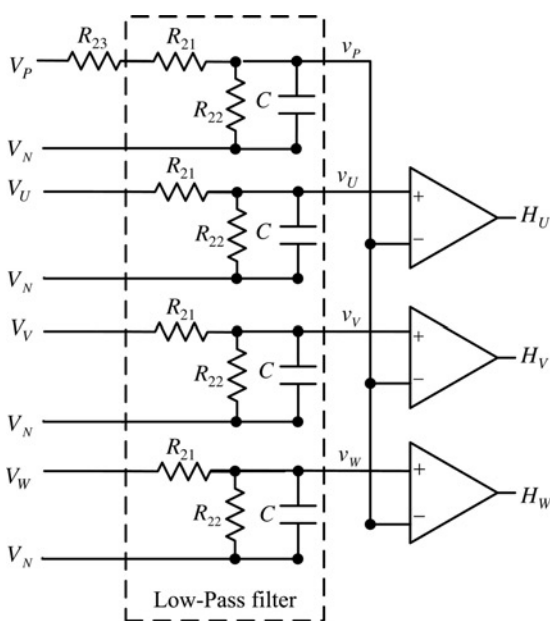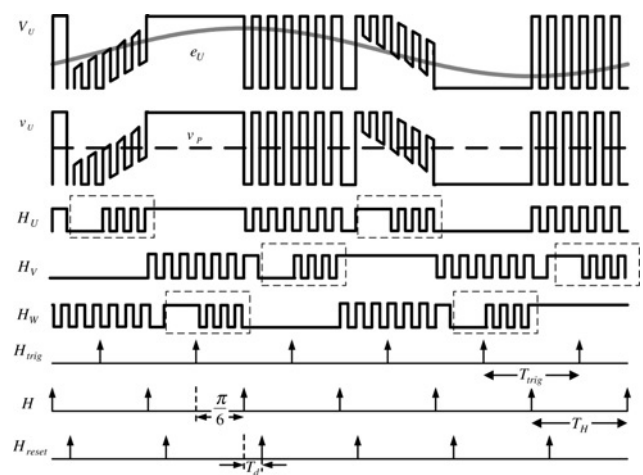

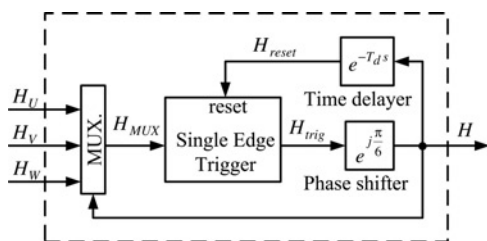**Figure 8** *Illustrated waveforms for BEDC-II*

Figure 9 *Commutation signal generator for BEDC-II*

4.3 Commutation signal generator

The block of commutation signal generator for BEDC-II is plotted in Fig. 9 where a multiplexer is used to select the unexcited-phase position signal by commutation signal H. To operate BDCM normally, we should commutate current adequately at $(30° + k × 60°)$ position behind ZCPs of back-EMFs. It implies that the detections of ZCPs from BEDC-II cannot directly be used as commutation signals. Thus, unlike the commutation signal generator of BEDC-I in Fig. 5, a phase shifter should be included in the commutation signal generator of BEDC-II.

Because of the conduction of freewheeling diodes at the current commutation, the terminal voltage would be equal to V_{dc} or zero until line current returns to zero, which may result in the failure detection of ZCPs. Therefore in the commutation signal generator, the single-edge-trigger function is designed to capture the first edge-change of signal H_{MUX} and then, hold until the coming of active reset signal H_{reset}. The reset signal H_{reset} is obtained from T_d-delayed commutation signal H. Finally, by shifting the trigger signal H_{trig} with $\pi/6$, we can obtain the desired commutation signal H.

4.4 Position-dependent load torque

In general-purpose DSP/MCU, the implementation of $\pi/6$ phase shifter is not easy and would take some fixed execution time. Generally speaking, the error of phase shifter at high speed is larger than the near zero error at low speed. It means that the phase shifter would introduce some error into the current commutation for BEDC-II, particularly at high speed and we should pay more attention to the performance of commutation signal generator as shown in Figs. 5 and 9. Therefore to reduce the effect of phase shifter on commutation signal, many specific MCUs for the purpose of sensorless square-current operations have been developed [3, 14].

Since BEDC-II is designed based on the equality in (9), the ZCPs of back-EMFs can be exactly detected even under varying speed resulting from position-dependent load torque. Therefore the performance of BEDC-I dominates the performance of sensorless square-current operation. But for BEDC-II, its cooperating commutation signal generator would degrade the performance of sensorless square-current operation.

5 Simulation results

To evaluate the position detecting error $\Delta\theta$ of BEDC-I and BEDC-II, some simulation results are provided in this section. According to the circuit analysis in (1)–(11), the simulated parameters for various BEDCs are listed as

$$R_{11} = 470 \text{ k}\Omega, R_{12} = 47 \text{ k}\Omega, R_{13} = 30 \text{ k}\Omega$$
$$R_{14} = 2 \text{ k}\Omega, C_{11} = C_{12} = 2.2 \text{ μF}, C_{13} = 470 \text{ nF}$$
$$R_{21} = 300 \text{ k}\Omega, R_{22} = 12 \text{ k}\Omega, R_{23} = 312 \text{ k}\Omega, C = 330 \text{ pF}$$
$$(12)$$

To evaluate the position detecting errors of both BEDCs fairly and avoid the error from commutation signal generators, the operations of BDCMs in simulation are operated with 'sensor-feedback'. That is, the commutation signal H is directly generated from the position sensor. In addition, PWM duty ratio in simulation is given, not automatically tuned by speed loop. It follows that the simulated position detecting errors $\Delta\theta$ are introduced only from BEDCs. The parameters of simulated 4-pole BDCM are listed in Table 2.

5.1 Constant load torque

When a BDCM is operating with constant load torque, the motor speed can be seen as fixed and the resulting position error is constant. For constant load torque 1 N-m, the obtained average detecting errors $\Delta\theta$ by keeping the PWM duty ratio fixed from 20 to 80% can be tabulated in Table 3. From Table 3, we can find that the position detection error $\Delta\theta$ of BEDC-II is small and near constant during the speed range. But for BEDC-I, the position detection error $\Delta\theta$ varies from negative value to positive value because of its frequency-dependent (i.e. speed-dependent) performance.

Table 2 Simulated parameters

stator resistance	0.7 Ω
stator inductance	$L_q = 10.5$ mH, $L_d = 4$ mH
voltage constant (line-to-line)	23.63 mV_{rms}/rpm
speed range	$\omega_{r,Low} = 1200$ rpm, $\omega_{r,High} = 6000$ rpm
motor inertia	0.0004 kg $-$ m^2
DC link voltage	300 V
PWM frequency	5 kHz
constant load torque	1 N $-$ m

Table 3 Position detection error $\Delta\theta$ at constant load torque

Duty $\Delta\theta$	20%	30%	40%	50%	60%	70%	80%
	1280 rpm	2000 rpm	2740 rpm	3470 rpm	4210 rpm	4940 rpm	5690 rpm
BEDC-I	$-16.5°$	$-9.17°$	$-3.12°$	$2.155°$	$6.685°$	$11.99°$	$16.43°$
BEDC-II	$3.426°$	$0.29°$	$1.074°$	$1.01°$	$0.894°$	$1.082°$	$0.66°$

5.2 Position-dependent load torque

In the following simulation, the position-dependent load torque is given as

$$T_{\mathrm{L}} = 1 + 0.5\sin\theta_{\mathrm{r}} \ (\mathrm{N-m}) \qquad (13)$$

where θ_{r} is the rotor position and its average torque is also equal to the same value 1 N-m as the constant load torque in the previous section. By keeping the PWM duty ratio fixed at 20%, 50% and 80%, the simulated position detecting errors $\Delta\theta$ are plotted in Fig. 10*a* and 10*b*, respectively.

From Fig. 10*a*, we can find that position detecting error $\Delta\theta$ of BEDC-I changes with the rotor position θ_{r}, especially at low speed. At high speed, the speed variation due to position-dependent load torque becomes small and thus the position detecting error $\Delta\theta$ is almost constant under various rotor positions θ_{r}. The simulated errors shown in Fig. 10*b* indicate that both position detecting error of BEDC-II and its variation are small.

5.3 Comments

The error resulting from commutation signal generator has been removed in the above simulation. Obviously, the simulated results in Table 3 and Fig. 10 indicate that BEDC-II is better than BEDC-I during the entire speed range. However, the performance of sensorless operation is dependent on the commutation error, not only on the position detecting error of BEDC. It means that the performance of sensorless operation with BEDC-II may or may not be better than that with BEDC-I during various speeds.

6 Experimental results

To evaluate the low-speed performances of various BEDCs under position-dependent load torque, an experimental system is set up in the laboratory. It mainly consists of two identified BDCMs coupled to each other as plotted in Fig. 1, an aluminium disk and a copper cylinder where the cylinder is fixed on the disk as shown in Fig. 11. All the motors and the disk are coupled to the unique shaft. The circuit parameters of used BEDCs and motor parameters of two used BDCMs in experiments are the same as (12) and Table 2.

The two coupled BDCMs can be seen as a Motor-Generator (M-G) set where the Generator-end terminals are connected to the Y-connected resistors as shown in Fig. 1 to provide a constant load torque regardless of the rotor position. Besides, the copper cylinder on the disk contributes to a position-dependent load torque because of the unified direction of the gravity force. Since the weight
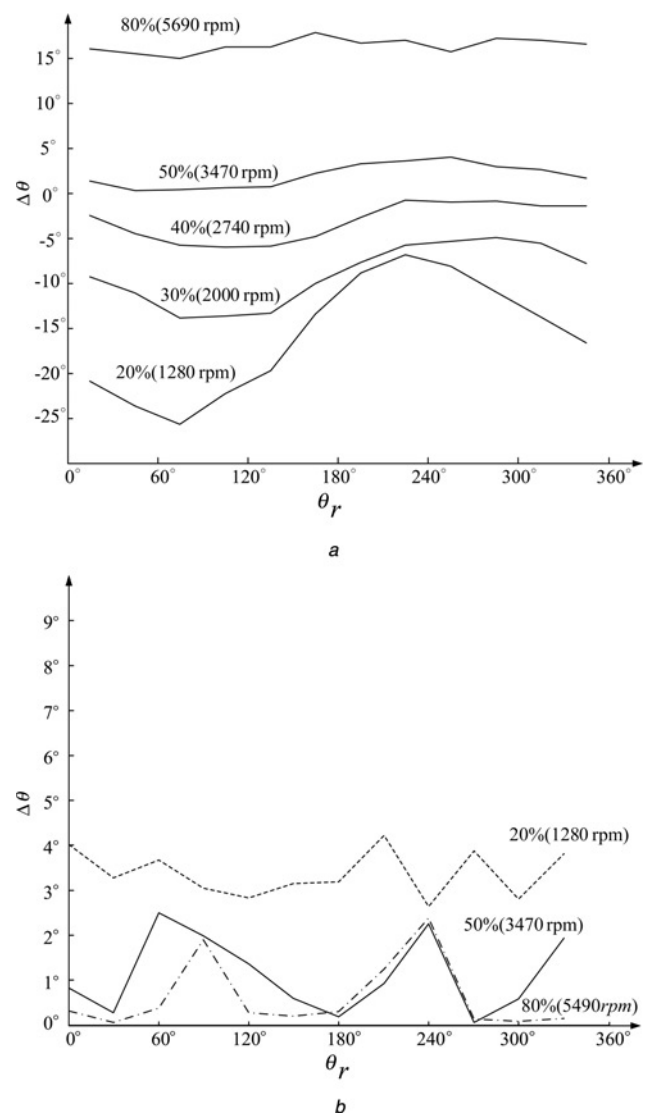
Figure 10 *Simulated position detecting error with position-dependent load torque for*

a BEDC-I
b BEDC-II
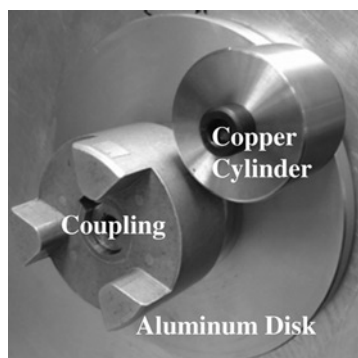
Figure 11 *Experimental position-dependent load torque*

of copper cylinder is 203.58 g and its distance to the couple is 5 cm, the resulting peak torque is near 0.2 N-m.

As shown in the dashed line of Fig. 1, all sensorless functions including commutation signal generator, speed estimation, speed controller and switching signal generator are digitally implemented in general-purpose MCU. The BDCM speed ω_r is estimated by the period T_H of the signal H

$$\omega_r = \frac{1}{6T_H} \times \frac{60}{P/2} = \frac{20}{PT_H} \text{(rpm)} \tag{14}$$

The $\pi/6$ phase shifter is implemented by delaying the input signal H_{trig} with its half period T_{trig}. It is noted that the smaller the period T_{trig} is, the larger is the delay error caused by constant MCU execution time. Therefore the performance of commutation signal generators cannot be neglected in evaluating the performance of sensorless control.

At low speeds (i.e. near $\omega_{r,Low}$), the error due to fixed execution time is relatively small and can be neglected. Therefore the current commutation error is dominated by the position detecting error of BEDC. The smaller position error may lead to small current commutation error and thus small current and small power at low speed.

Consequently, we turn to record the input power with various BDCM speed and position-dependent load torques. Relatively small input power implies that small position detecting error exists in the experiment. The Generator-end terminals are connected to three 5 Ω resistors to run at a relatively low speed.

With position-dependent load torque, the recorded BDCM speed ω_r and input power P_{in} for BEDC-I and BEDC-II are plotted in Fig. 12. From Fig. 12, we can find that with the same BDCM speed, less power is required for BEDC-II than that for BEDC-I. Thus, BEDC-II actually yields better performance than BEDC-I at low speeds.
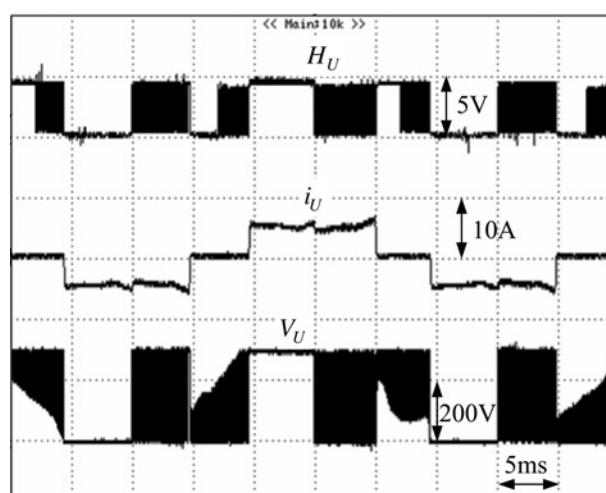
With the increase in speed, the fixed execution time would result in a relatively large phase error. Therefore the
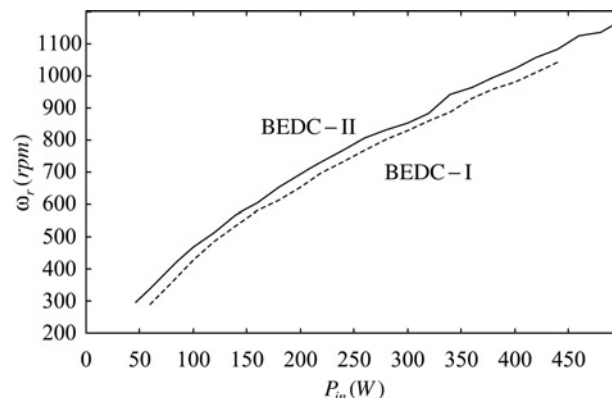
Figure 12 *BDCM speed and input power with position-dependent load torque*
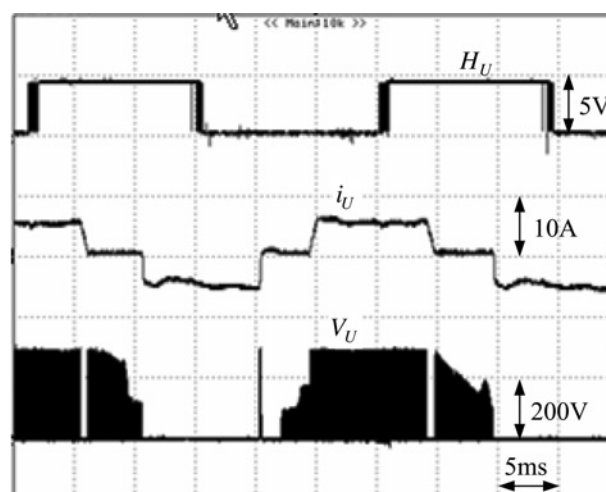
a

b

Figure 13 *Experimental waveforms of position signal H_U, motor winding current i_U and terminal voltage V_U for*

a BEDC-I with FUPWM
b BEDC-II with FLagPWM

commutation error for BEDC-II may be larger than that for BEDC-I at high speed (i.e. near $\omega_{r,High}$), though BEDC-II is better than BEDC-I from simulation results.

At low speed (i.e. near $\omega_{r,Low}$), the detection error of BEDC can be well judged in the experiment. At high speed (i.e. near $\omega_{r,High}$), it is hard to separate the BEDC error from the commutation error. Therefore the authors carefully claim that BEDC-II performs better than BEDC-I at low speeds, especially with position-dependent load torque.

The measured waveforms of position signal H_U, current i_U and terminal voltage V_U for BEDC-I with FUPWM and BEDC-II with FLagPWM at near 1000 rpm are plotted in Fig. 13a and 13b, respectively. From Table 3, the simulated position error is about $16°$ at about 1000 rpm. Therefore BDCM sensorless control with BEDC-I work well with large position error. However, from the view of the simplicity of commutation signal generator, BEDC-I possesses competitive advantage in the high-speed application of sensorless control.

7 Conclusion

In this paper, the low-speed performances and comparisons of two BEDCs and their sensorless controls are studied under position-dependent load torque. The implementation of commutation signal generation is the only difference between the sensorless control of BEDC-I and BEDC-II. From the analysis, the implementation of sensorless control for BEDC-I is simpler than that for BEDC-II. However, BEDC-II yields less position detecting error than BEDC-I, especially at low speed. The simulation and experimental results also demonstrate the analysis result. It follows that BEDC-II is suitable in low-speed application of BDCMs.

8 Acknowledgment

9 References

[1] ACARNLEY P.P., WATSON J.F.: 'Review of position-sensorless operation of brushless permanent-magnet machines', *IEEE Trans. Ind. Electron.*, 2006, **53**, (2), pp. 352–362

[2] IIZUKA K.: 'Microcomputer control for sensorless brushless motor', *IEEE Trans. Ind. Appl.*, 1985, **27**, (3), pp. 595–601

[3] CHEN H.C., CHANG Y.C., HUANG C.K.: 'Practical sensorless control for inverter-fed BDCM compressors', *IET Electr. Power Appl.*, 2007, **1**, (1), pp. 127–132

[4] LI Q., WANG R.: 'Study on rotor position detection error in sensorless BLDC motor drives'. Proc. IPEMC'06, 2006, vol. 3, pp. 1–5

[5] DAMODHARAN P., VASUDEVAN K.: 'Indirect back-EMF zero crossing detection for sensorless BLDC motor operation'. Proc. PEDS'05, 2005, vol. 2, pp. 1107–1111

[6] CHEN C.H., CHEN M.Y.: 'Design of a multispeed winding for a brushless DC motor and its sensorless control', *IEE Proc. Electr. Power Appl.*, 2006, **153**, (6), pp. 834–841

[7] SU G.J., MCKEEVER W.: 'Low-cost sensorless control of brushless DC motors with improved speed range', *IEEE Trans. Power Electron.*, 2004, **19**, (2), pp. 296–302

[8] KIM D.K., LEE K.W., KWON B.I.: 'Commutation torque ripple reduction in a position sensorless brushless DC motor drive', *IEEE Trans. Power Electron.*, 2006, **21**, (6), pp. 1762–1768

[9] KANG Y., LEE S.B., YOO J.: 'A microcontroller embedded AD converter based low cost sensorless technique for brushless DC motor drives'. Proc. IEEE IAS'05, 2005, vol. 3, pp. 2176–2181

[10] DELALEAU E., STANKOVIC A.M.: 'Modeling and simulation of the induction motor with position-dependent load torque'. Proc. 42nd Conference on Decision and Control, 2003, pp. 6212–6217

[11] CHEN H.C., HUANG C.K.: 'Robust speed control for position-dependent load torque'. Proc. PESC'07, 2007, pp. 2739–2744

[12] KIM K.H., YOUN M.J.: 'Performance comparison of PWM inverter and variable DC link inverter schemes for high-speed sensorless control of BLDC motor', *Electron. Lett.*, 2002, **38**, (21), pp. 1294–1295

[13] WANG C.C., SUNG G.N., FANG K.W., TSENG S.L.: 'A low-power sensorless inverter controller of brushless DC motors'. Proc. ISCAS'07, 2007, pp. 2435–2438

[14] SHAO J., NOLAN D., HOPKINS T.: 'Improved direct back EMF detection for sensorless brushless DC (BLDC) motor drives'. Proc. APEC'03, 2003, pp. 300–305